Electronic Supplementary Material (ESI) for Journal of Materials Chemistry A.

Supporting Information

MOF-Derived α-NiS Nanorods on Graphene as an Electrode for High-Energy-Density Supercapacitors

Chong Qu‡[1,2], Lei Zhang‡[2], Wei Meng‡[1], Zibin Liang[1], Dai Dang[2], Shuge Dai[2], Bote Zhao[2], Bingjun Zhu[1], Hassina Tabassum[1], Song Gao[1], Hao Zhang[1], Wenhan Guo[1], Ruo Zhao[1], Xinyu Huang[1], Meilin Liu[2], and Ruqiang Zou[1]**

1 Beijing Key Laboratory for Theory and Technology of Advanced Battery Materials, Department of Materials Science and Engineering, College of Engineering, Peking University, Beijing 100871, China

2 School of Materials Science and Engineering, Georgia Institute of Technology, 771 Ferst Drive, Atlanta, GA 30332, United States

‡These authors contributed equally to this work.

Basic characterizations

The crystallographic structures of the materials were obtained using a Bruker D8 advanced diffractometer powder X-ray diffraction (PXRD) with an X'celerator module and Cu Kα (λ = 1.54050 Å) radiation at room temperature, with a step size of 10° in 2θ. Raman spectra were obtained using a Renishaw spectromicroscopy system equipped with a 20× objective optical microscope. The microstructure and morphology were examined by using a field emission scanning electron microscope (FE-SEM) (Hitachi S-4800) equipped with a Bruker Quantax energy dispersive spectrometer (EDS). Transmission electron microscope (TEM) images were taken on FEI Tecnai F20 and F30 microscopes. Elemental analysis was performed on a Vario EL Elemental Analyzer. Surface characterization of elemental electronic states was measured by X-ray photoelectron spectroscopy (XPS) (Kratos Axis Ultra Imaging Photoelectron Spectrometer). The instrument was equipped with a monochromatic Al-Kα X-ray source (hν=1468.7 eV). The nitrogen isotherms of the materials were measured within the pressure range 0-1 atm at 77K using a Quadrasorb system from a Quantachrome Autosorb-IQ gas adsorption analyzer. Applying the Brunauer-Emmett-Teller (BET) model and quenched solid state functional theory (QS-DFT) to these isotherms, specific surface areas and pore sizes distribution were determined for each material.

Electrochemical measurement

The electrochemical measurements were carried out by using a Zahner Zennium electrochemical workstation in case of both three-electrode configuration and two-electrode device. For the working electrode of three-electrode system, a mixture slurry containing of 80 wt% active materials, 10 wt% Super P and 10 wt% PTFE binder was prepared then rolled with the assistance of ethanol to form a uniform film with a typical areal mass of approximately 2.5 mg cm^{-2}. The film electrode was then pressed between two nickel foam, and dried under vacuum at 80 ˚C for 12 h. A platinum mesh electrode and an Ag/AgCl electrode prefilled with saturated KCl aqueous solution were used as the counter and the reference electrodes, respectively. The cyclic voltammograms (CV) were acquired in a potential range between 0 and 0.55 V at different scan rates, and the charge-discharge processes were performed between 0 and 0.5 V at different current densities in a 2 M KOH aqueous electrolyte. Based on the galvanostatic discharge curve, the specific capacity Q (C g^{-1}) of the battery-type R-NiS/rGO was calculated as follows:

$$Q = i_m \Delta t \qquad \text{(S1)}$$

where i_m=I/m (A g^{-1}) is the current density, m is the mass of the active material, Δt(s) is the discharge time.

The cyclic stability was evaluated by galvanostatic charge-discharge measurements at a current density of 20 A g^{-1}.

The electrochemical measurements of the two-electrode device containing R-NiS/rGO as positive electrode and C/NG-A as negative electrode (-1-0 V) with separator of MPF30AC-100 (Nippon Kodoshi Corporation, Kochi, Japan) in a split test cell (MTI Corporation) configuration were carried out in a 2 M KOH electrolyte. The negative electrode film was prepared with the same method described above with 90 wt% C/NG-A and 10 wt% PTFE binder. The mass ratio of positive electrode to negative electrode is determined according to charge balance theory ($q^+ = q^-$). Based on the CV results from three-electrode system,

$$q = \int imdV/v \qquad \text{(S2)}$$

where q represents the charge, m is the mass of the active material, and $\int idV/v$ is the integral area from CV.

In order to achieve charge balance, $m^{+}\cdot\left(\int\frac{idV}{v}\right)_{+}=m^{-}\cdot\left(\int\frac{idV}{v}\right)_{-}$, thus,

$$m^{+}:m^{-}=\left(\int\frac{idV}{v}\right)_{-}:\left(\int\frac{idV}{v}\right)_{+} \qquad \text{(S3)}$$

The CV was acquired in a potential range between 0 and 1.6 V at different scan rates, and the charge-discharge processes were performed by cycling the potential from 0 to 1.6 V at different current densities. The cyclic stability was evaluated by galvanostatic charge-discharge measurements at a current density of 20 A g^{-1}.

The specific capacitance was calculated from the galvanostatic charge-discharge measurements using the following equation,

$$C=\frac{2i_m\int Vdt}{V^2\Big|_{V_i}^{V_f}} \qquad \text{(S4)}$$

C represents the galvanostatic charge-discharge (GCD) specific capacitance. $\int Vdt$ is the integral current area, where V is the potential with initial and final values of V_i and V_f, respectively. i_m $=I/m$ is the current density, where I is the current and m is the mass of active materials.

The energy density E (Wh kg^{-1}) and power density P (W kg^{-1}) in Ragone plot were calculated with the following equations,

$$E = \frac{1}{2} \cdot \frac{C \cdot \Delta V^2}{3.6} \quad \text{(S5)}$$

$$P = 3600 \cdot \frac{E}{\Delta t} \quad \text{(S6)}$$

Where C is the specific gravimetric capacitance (F g^{-1}), ΔV is the potential window (V), and Δt is the discharge time (S).

Density functional theory (DFT) calculation

Density functional theory calculations were performed within VASP (Vienna ab-initio Simulation Package) {Efficient iterative schemes for ab initio total-energy calculations using a plane-wave basis set}. The generalized gradient approximation parameterized by Perdew, Burke and Ernzerhof under projector augmented wave function {Generalized gradient approximation made simple} was applied to pseudo-potentials of Ni and S. Three surface slabs were constructed and visualized via VESTA, with a 15 Å vacuum space for each one. (110), (101) and (102) slabs have 64, 128 and 160 atoms per supercell. Energy was sampled by $1 \times 1 \times 1$ reciprocal space mesh centered at gamma point. To ensure convergence, an energy cut-off of 400 eV was chosen to reach the energy and force accuracy of 1E-6 eV and 0.01 eV/ Å. Energy correction {Periodic boundary conditions in ab-initio calculations} due to polarization of surface slab was considered for all three slabs, as well as charged hydroxyl, i.e. OH-. The surface energy was calculated via the equation shown below:

$$E_{sur} = (E_{slab} - nE_{unit-bulk})/2A \quad \text{(S7)}$$

where E_{sur} is the surface energy, E_{slab} and $E_{unit-bulk}$ is the total energy of slab super-cell and bulk unit-cell, n is the multiplicity of slab cell over unit cell, A is surface area of the slab.

The adsorption energy of OH- was calculated via the equation shown below:

$$E_{ads} = E_{*-OH} - E_{slab} - E_{OH^-} \quad \text{(S8)}$$

where E_{*-OH} is the total energy of NiS slab with hydroxyl group adsorbed on one surface Ni site, E_{slab} is the total energy of slab super-cell, and E_{OH^-} is the total energy of an isolated OH^-.

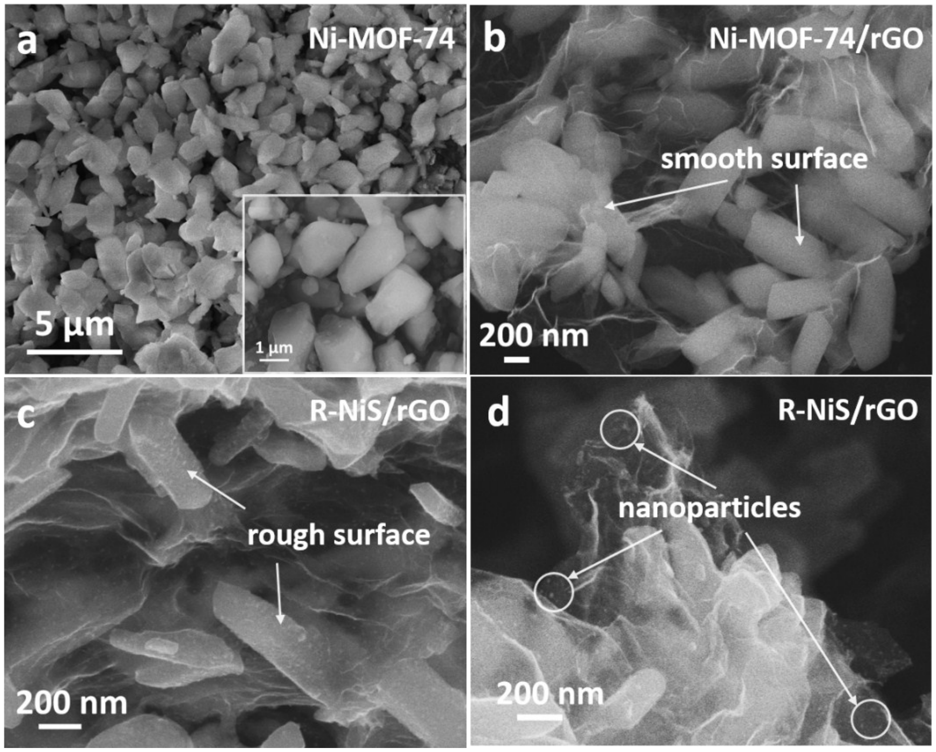

Figure S1. SEM images of (a) Ni-MOF-74 bulk materials, (b) Ni-MOF-74/rGO hybrid nanostructure, and (c-d) R-NiS/rGO nanohybrids. The arrows in (b), (c), and (d) indicate different surface morphologies between Ni-MOF-74/rGO and R-NiS/rGO.

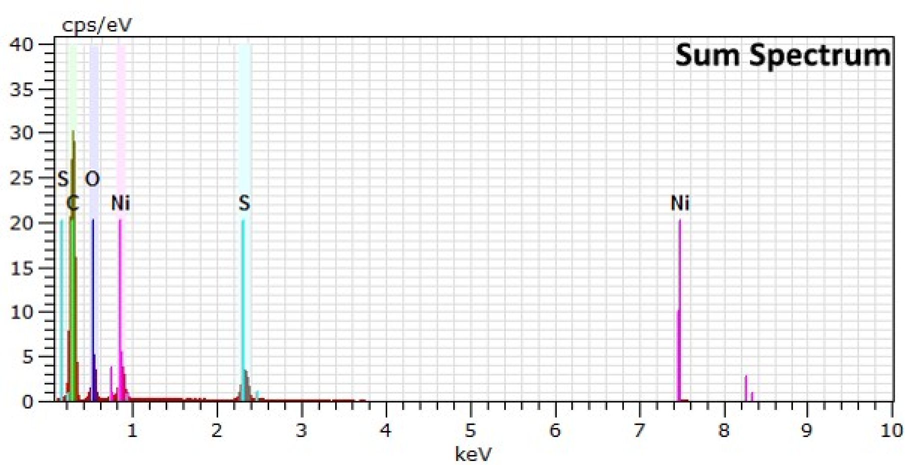

Figure S2. EDS sum spectrum of the R-NiS/rGO.

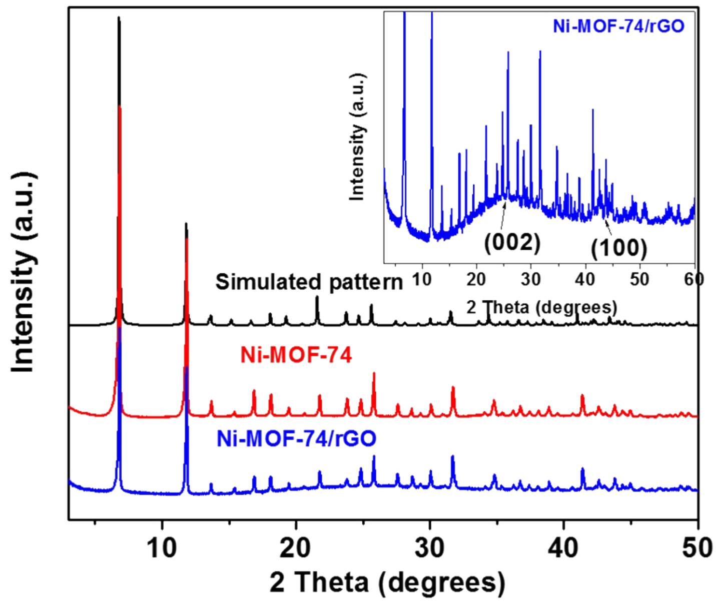

Figure S3. PXRD patterns of the as-synthesized Ni-MOF-74, Ni-MOF-74/rGO, and the simulated MOF-74, inset is the enlarged Ni-MOF-74/rGO XRD pattern.

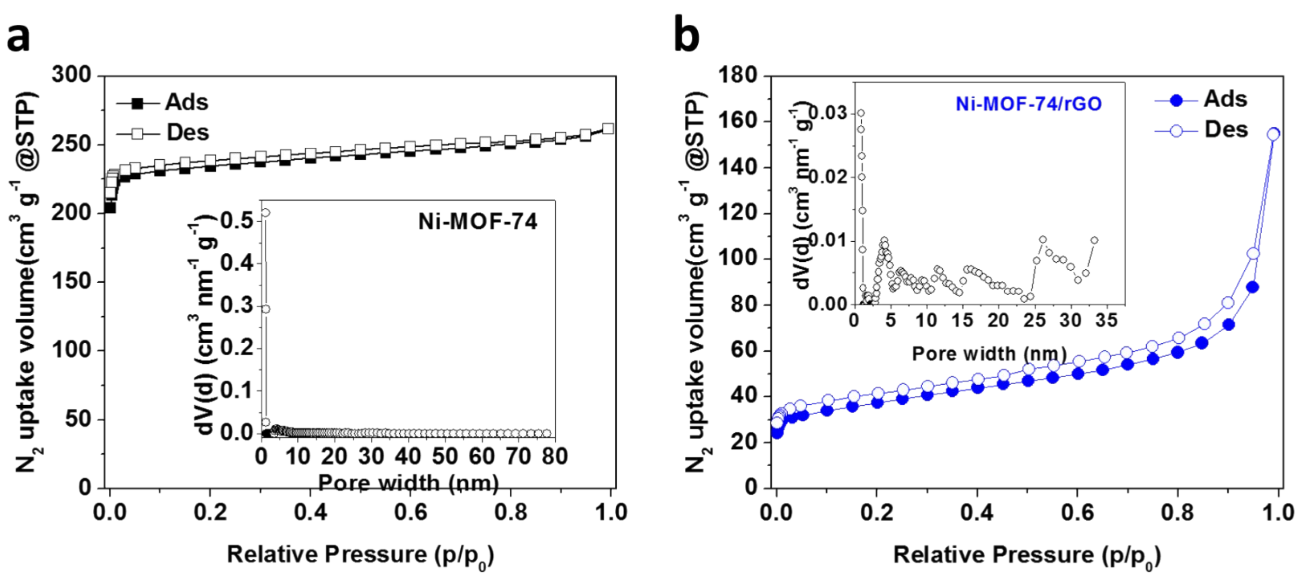

Figure S4. N_2 adsorption-desorption isotherms and corresponding pore size distribution plot (inset) of a) Ni-MOF-74 and b) Ni-MOF-74/rGO.

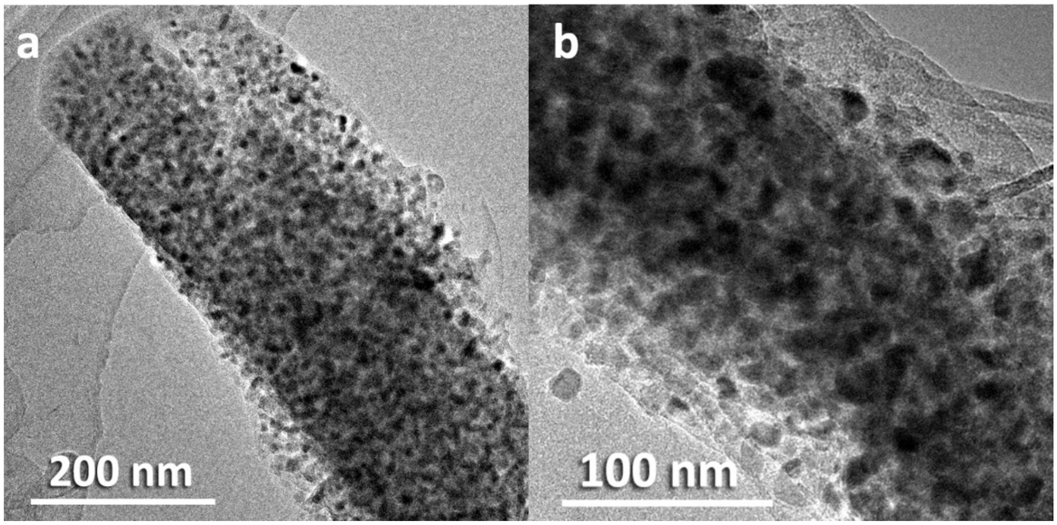

Figure S5. TEM images of the NiS nanorod decorated on the graphene sheets.

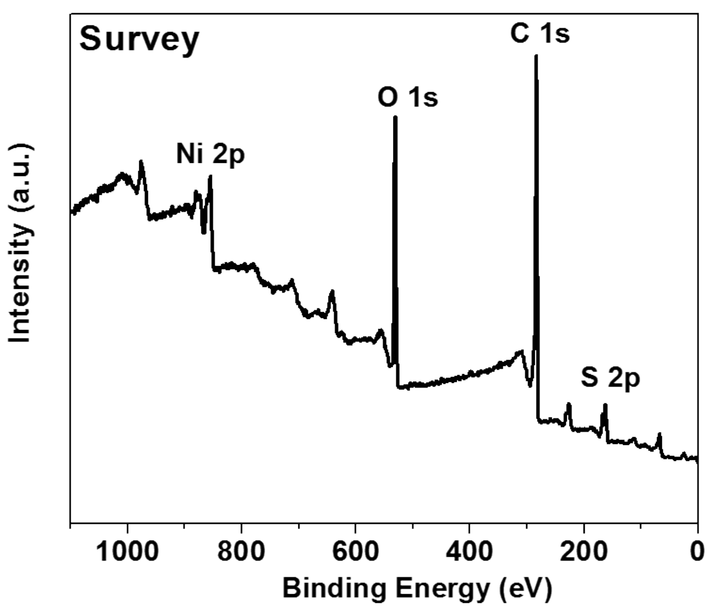

Figure S6. XPS survey spectrum of the R-NiS/rGO.

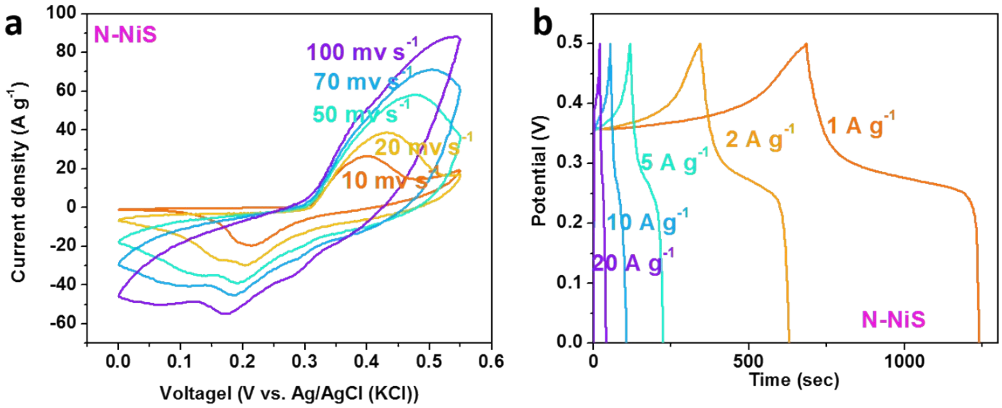

Figure S7. a) CV curves of N-NiS, b) GCD curves of N-NiS.

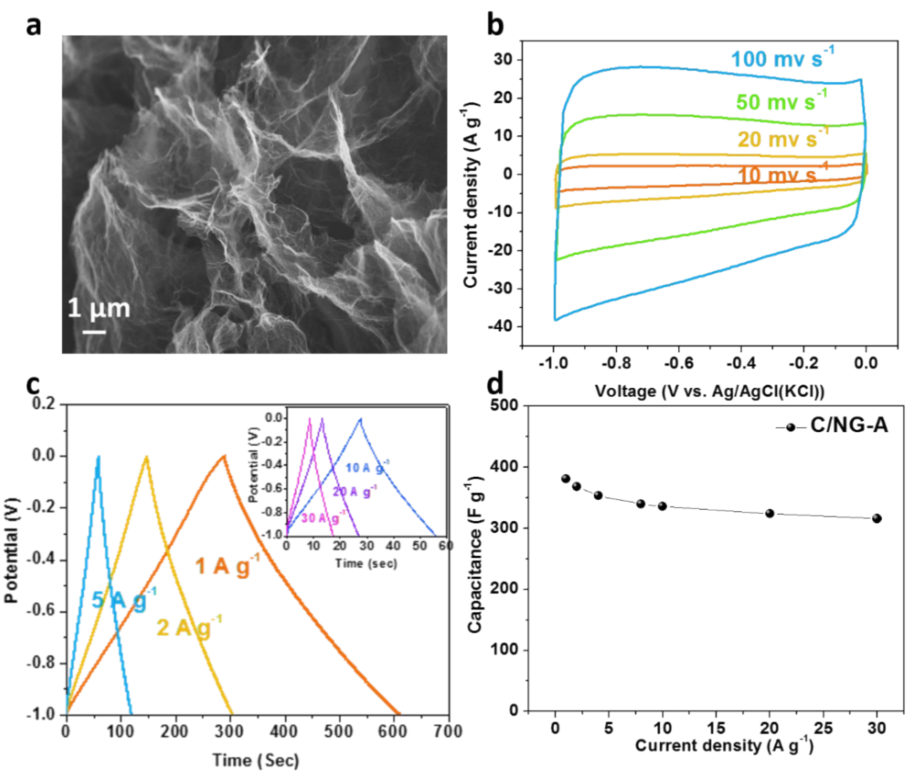

Figure S8. a) SEM image of the C/NG-A, b) CV curves of the C/NG-A at different scan rates, c) GCD curves of the C/NG-A at different current densities, and d) Specific capacitances and rate capability of the C/NG-A.

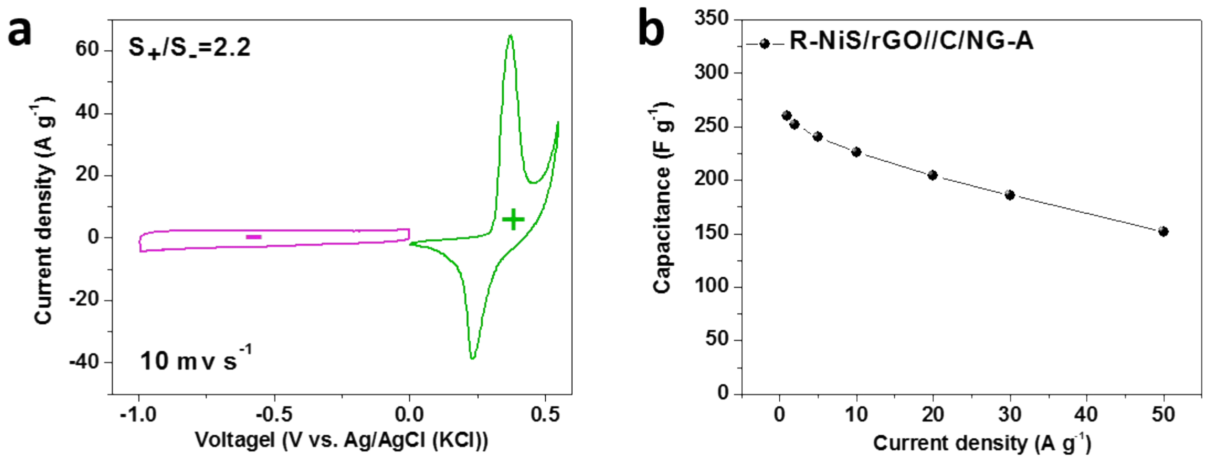

Figure S9. a) CV comparison between the positive and negative electrodes of the R-NiS/rGO//C/NG-A device, b) Specific capacitances and rate capability of the R-NiS/rGO//C/NG-A hybrid supercapacitor.

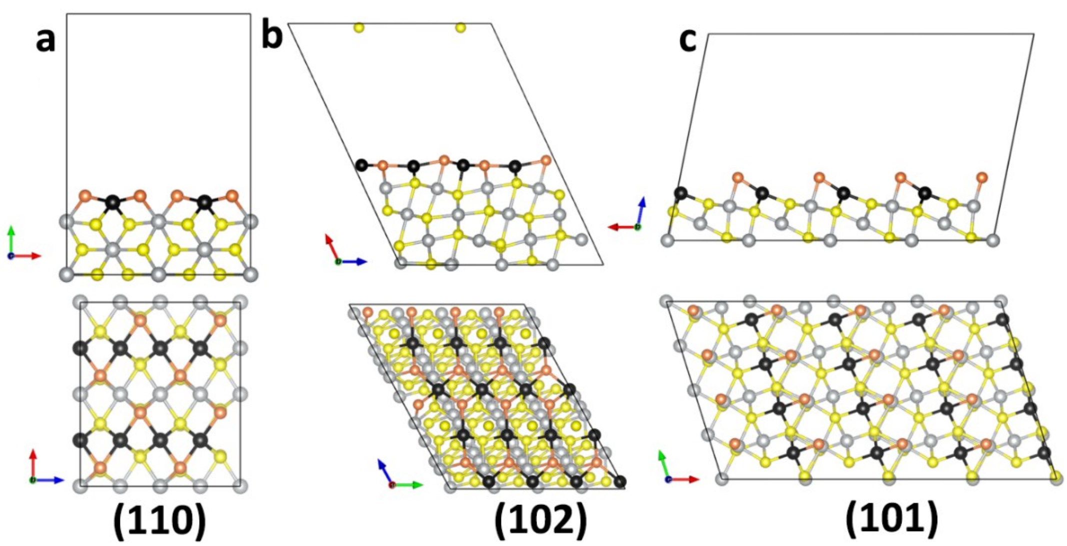

Figure S10. α-NiS slabs: (a) (110), (b) (102), and (c) (101) with surface exposed to vacuum. Black and copper balls are surface Ni and S atoms, while silver and yellow ones are the rest Ni and S atoms. Red, green and blue arrows are lattice vectors a, b and c. Upper pictures are side view; lower picture is vertical view.